



CrossMark
 click for updates

Cite this: *RSC Adv.*, 2015, 5, 59976

Gas sensors based on ultrathin porous Co₃O₄ nanosheets to detect acetone at low temperature

Ziyue Zhang,^{ab} Zhen Wen,^{ab} Zhizhen Ye^{ab} and Liping Zhu^{*ab}

Using a facile two-step process, including a hydrothermal technique and subsequently controlled annealing of the precursor, ultrathin porous Co₃O₄ nanosheets can be synthesized. The gas sensor based on the porous Co₃O₄ nanosheets shows a superior acetone gas-sensing performance at a low operating temperature of 150 °C. The gas response to 100 ppm acetone reached 11.4, and exhibited good reproducibility. In addition, the detection limit of the Co₃O₄ nanosheet sensor is lower than 1.8 ppm, which is the diagnostic criteria exhaled from diabetes. What's more, the sensor exhibited good stability when tested over 2 months. The outstanding gas-sensing properties were explained by a typical p-type semiconductor behavior with an ultrathin porosity structure as well as a large specific surface area of Co₃O₄ nanosheets.

Received 8th May 2015
 Accepted 25th June 2015

DOI: 10.1039/c5ra08536e

www.rsc.org/advances

Introduction

With the increasingly prominent issues concerning food and the environment, people are placing much more emphasis on the advanced diagnosis of their health conditions. Regular physical examinations, consisting of ultrasonication, electrocardiography and irradiation as well as testing blood and urine,¹ are time and resource consuming and inconvenient. During the past few years, a testing approach utilizing the analysis of exhaled breath from human bodies to make an initial judgment on their physical condition has been proposed by researchers.² Basically, the exhaled breath of healthy people contains carbon dioxide, nitrogen, vapour, rare gases and various organic gases produced during the metabolic process.^{3,4} If a certain gas concentration is beyond its normal range, it could mean that the human is ill.⁵ For instance, diabetes, asthma, heart disease, kidney malfunction and chronic obstructive pulmonary disease are closely related to the concentration of exhaled acetone, nitrogen monoxide, pentane, ammonia and carbon monoxide, respectively.⁶ Among these illnesses, diabetes is the most common chronic disease at present. If it can be found at an early stage, people with pre-diabetes can sharply lower their chances of developing the disease.^{7,8} Nowadays, gas chromatographic detection technology, selected ion flow tube mass spectrometry and cavity ring down spectroscopy are the most common diagnostic techniques used to detect acetone in exhaled breath.^{9–12} But, in addition to these detection technologies, gas sensors have great potential to be used as acetone

testing instruments in the future, due to their advantages, such as being small, portable and low-cost.

Due to the inherent advantages of gas sensors, such as being portable, cheap and suitable for daily use,^{13–16} people have begun to consider using gas sensors in the analysis of exhaled breath.^{17,18} For example, Marco Righettoni *et al.* developed gas sensors based on Si-doped WO₃ to analyse breath acetone for diabetes detection at 400 °C,¹⁹ Li *et al.* synthesised co-doped ZnO nanofiber-based gas sensors to detect acetone at 360 °C,²⁰ Song *et al.* produced Ce doped SnO₂ hollow spheres as acetone gas sensors at 250 °C,²¹ and Zhou *et al.* developed acetone gas sensors based on porous ZnO/ZnCo₂O₄ hollow spheres at 275 °C.²² However, in order to achieve their optimal sensing performances, these sensors usually have low sensitivity and need higher working temperatures, which not only shortens sensor lifetime but also increases the cost of practical applications. Thus, the large-scale application of these sensors in our daily life to detect diabetes is limited. In our previous work, we reported a Co₃O₄ nanorod array-based ethanol gas sensor with a low operating temperature.^{23–25} Therefore, we attempted to prepare a kind of Co₃O₄ sensor to detect acetone for diagnosing diabetes at a low operating temperature.

In this work, we present the fabrication of an ultrathin porous Co₃O₄ nanosheet-based gas sensor with high-performance for selective acetone detection at a relatively low temperature. The characterization techniques used on of the Co₃O₄ nanosheets include scanning electron microscopy (SEM), thermogravimetric analysis (TGA), X-ray diffraction (XRD), transmission electron microscopy (TEM), high-resolution TEM (HRTEM) and Brunauer–Emmet–Teller (BET). Subsequently, the high-performance sensing properties of the gas sensor based on ultrathin porous Co₃O₄ nanosheets for acetone and the related gas-sensing mechanism will also be discussed.

^aSchool of Materials Science and Engineering, Zhejiang University, China

^bState Key Laboratory of Silicon Materials, Hangzhou 310027, People's Republic of China. E-mail: zlp1@zju.edu.cn; Fax: +86 571 87952625; Tel: +86 571 87952625

Experimental

Co₃O₄ nanomaterial synthesis

All chemicals were of analytical grade and used as purchased without further purification. The typical experiments were as follows: firstly, 0.02 mmol (0.125 g) poly(ethylene glycol)-*block*-poly(propylene glycol)-*block*-poly(ethylene glycol) was dissolved in a mixing solution with 16.5 mL ethanol and 1 mL high purity water (18.3 MΩ cm resistivity) under stirring at room temperature. Secondly, after obtaining a clarified solution, 0.5 mmol (0.07 g) hexamethylenetetramine and 0.5 mmol (0.125 g) cobalt acetate (C₄H₆O₄·Co·4H₂O) were added and stirred at 60 °C, then 13 mL ethylene glycol was added, until its colour changed from transparent to pink. Thirdly, the precursor solution was statically aged for 12 h. Fourthly, the homogeneous solution was transferred into a 50 mL Teflon-lined stainless steel autoclave, which was sealed and maintained at 170 °C for 2 h inside an electric oven. Fifthly, after cooling down to room temperature, the brown muddy solution in the autoclave was washed with distilled water and ethanol several times, in order to remove the free nanoparticle debris and the residual reactant. A light green powder was collected through washing/centrifugation (10 000 rpm, 3 min) and dried under vacuum at 60 °C for 12 h. Finally, a series of Co₃O₄ nanosheets were fabricated by annealing the as-prepared light green powder at 250 °C, 300 °C, 350 °C, 400 °C and 450 °C in air for 2 h (corresponding products denoted as S250, S300, S350, S400 and S450, respectively).

Characterization

The microstructures and morphologies of both the sample before annealing and the calcined products were examined using SEM (Hitachi, S-4800) with an accelerating voltage of 5 kV. The crystal phase identification was investigated using an XRD (Bede D1) system with Cu-K_{α1} radiation ($\lambda = 0.15406$ nm) over the 2θ range of 10–70°. TEM and HRTEM images were taken using a HRTEM analyser with an accelerating voltage of 200 kV. TGA (SDT Q600) was carried out under an air atmosphere at 10 °C min⁻¹ in the temperature range of 10–900 °C. Specific surface areas were computed from the results of the N₂ adsorption–desorption isotherms at 77 K (Micromeritics ASAP 3020).

Gas sensor fabrication

The as-prepared powder was mixed with a chitosan solution, in the appropriate weight ratio to get a 0.2 wt% CHIT solution, and ground in a mortar over time to form a paste. The paste was coated onto a polycrystalline alumina ceramic plate (8 mm × 4 mm, 0.5 mm thick) which had been plated with Ag–Pd finger regions (five pairs, both the width and distance were 200 μm) as electrodes to form a sensing film (with a thickness of ~6 μm, as shown in Fig. 1(a)). Finally, the samples were annealed at 60 °C for 12 h. The top view of the sample sensor is shown in Fig. 1(b), and Fig. 1(c) shows the schematic structure of sensor.

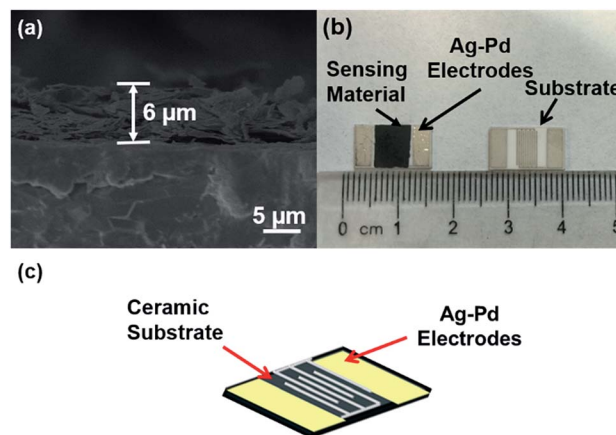


Fig. 1 (a) SEM image of a section of the sensor; (b) the top view of the sensor substrate and sample sensors; (c) a schematic structure of the sensor.

Gas-sensing measurements

The detailed gas-sensing experimental process can be found in our previous report.²⁶ We measured the gas sensing properties of the samples using an intelligent gas sensing analysis system (CGS-1TP, Beijing Elite Tech Co., Ltd, China). Two probes were pressed onto the sensor electrodes through adjusting their position in the analysis system. There is an external temperature control (from room temperature to 500 °C), which could easily adjust the sensor temperature with a precision of 1 °C. First of all, the sensor was preheated at different operating temperatures for about 1 h to achieve the stable resistances. Then through a rubber plug, the target gas was injected into the test chamber (18 L in volume) using a micro-injector. Our target liquid, *e.g.* acetone, was injected into the evaporator to form acetone vapour. Using the two fans in the analysis system, the saturated target gas was mixed with air (the relative humidity was about 50%). After the sensor resistance reached a new constant value, the test chamber was opened to recover the sensor in air. The gas response was designated as R_g/R_a , where R_g is the sensor resistance measured in the presence of the target gas and R_a in air. Response and recovery times were defined as the time needed to reach 90% of the total resistance change ($R_g - R_a$) on exposure to gas and air.

Results and discussion

Material characterization

The morphology and structure of the precursor obtained using the hydrothermal method were firstly investigated systematically. Fig. 2(a) indicates that the precursor is randomly shaped nanosheets with a smooth surface and are extremely thin (~30 nm). Fig. 2(b) shows the thermodecomposition behavior of the precursor, which implies that three decomposition steps exist: the first one appears below 200 °C, with a weight loss of about 5.5%. The weight loss is mainly due to the evaporation of adsorbed water in the sample. The second turning point appears at 310 °C, with a distinct weight loss of about 18.5%

between 200 °C and 310 °C, which is ascribed to the decomposition of the precursors, leading to the release of CO₂ and H₂O. Numerous fractured porous structures are formed during this stage, accompanying gas evolution and solid volume contraction. The third step appears after 310 °C, with the primary small nanoparticles growing into larger particles and the number of fractured porous structures decreasing gradually.

In order to find the most suitable annealing temperature for ideal ultrathin porous Co₃O₄ nanosheet-based gas sensors, the samples were annealed at different temperatures (from 250 °C to 450 °C). The XRD patterns of S250–S450 shown in Fig. 3(a) indicate that all of the samples are pure cubic Co₃O₄ phase. With the increasing annealing temperature, the intensity of the diffraction peaks increased, meaning that the grain size increased. The mean crystallite sizes were estimated from the (311) peak using the Scherrer formula, the grain sizes from S250 to S450 are 4.9 nm, 6.4 nm, 9.1 nm, 19.4 nm and 28.9 nm, respectively. Fig. 3(b)–(f) show the high-magnification SEM images of the ultrathin Co₃O₄ nanosheets obtained at different annealing temperatures. We can see that all of these samples are also random-shaped nanosheets, but compared with samples before annealing, these products have porous surfaces.

The pores on the surface were formed during the thermal treatment, because the generated CO₂ and H₂O (g) have escaped the samples. Comparing these SEM images, it can be found that both the size of the nanoparticles and pores throughout the nanosheets have gradually increased, with the increasing annealing temperature.

Further crystallographic properties were examined *via* TEM. Comparing the typical TEM images shown in Fig. 4(a)–(e), we can see that the cracked particles gradually grow, and the size of these particles become bigger as the annealing temperature increases from 250 °C to 450 °C, which is in agreement with that shown in the SEM images. What's more, the differences also influence the porosity of these Co₃O₄ nanosheets, including pore volume and pore density. From the HRTEM image shown in Fig. 4(f), the lattice fringe of $d = 0.466$ nm agrees well with the (111) crystallographic plane of the cubic Co₃O₄ phase.^{27–29}

N₂ sorption measurements were evaluated for characterization of the textural properties and inner architectures of the ultrathin Co₃O₄ nanosheets and gathering information about the specific surface area and pore size distribution. Fig. 5(a) displays the nitrogen adsorption and desorption isotherms of S250–S450, all of which reveal a typical type IV adsorption isotherm with a H3-type hysteresis loop at different relative pressure ranges. When elevating the annealing temperature, the corresponding specific surface areas of samples from S250 to S450 gradually decrease, and are 76.06 m² g⁻¹, 68.73 m² g⁻¹, 46.85 m² g⁻¹, 21.58 m² g⁻¹ and 19.49 m² g⁻¹, respectively. The pore diameter of the samples significantly increases with the increasing annealing temperature. However, according to

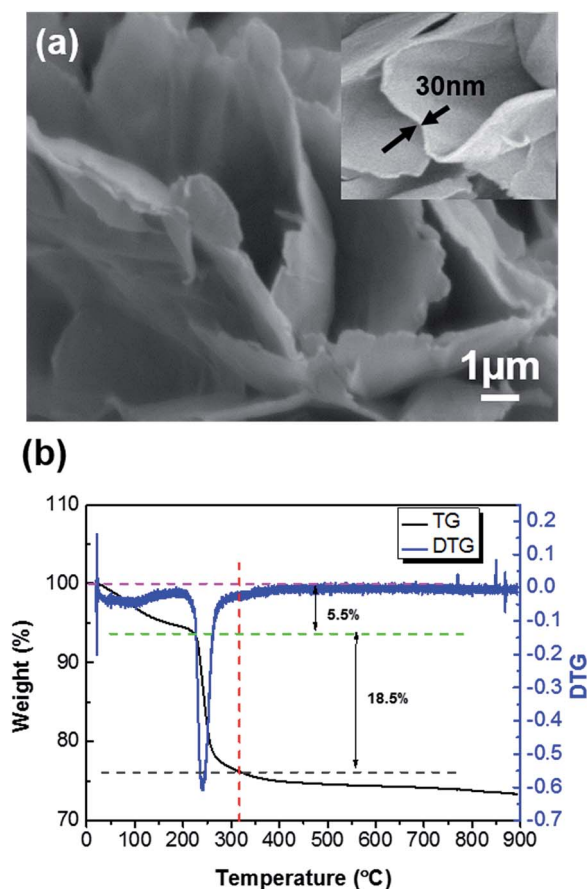


Fig. 2 Morphological and structural characterization of the precursor: (a) SEM images of the Co₃O₄ nanosheets; (b) TGA/DTG curves under air with a ramp of 10 °C min⁻¹.

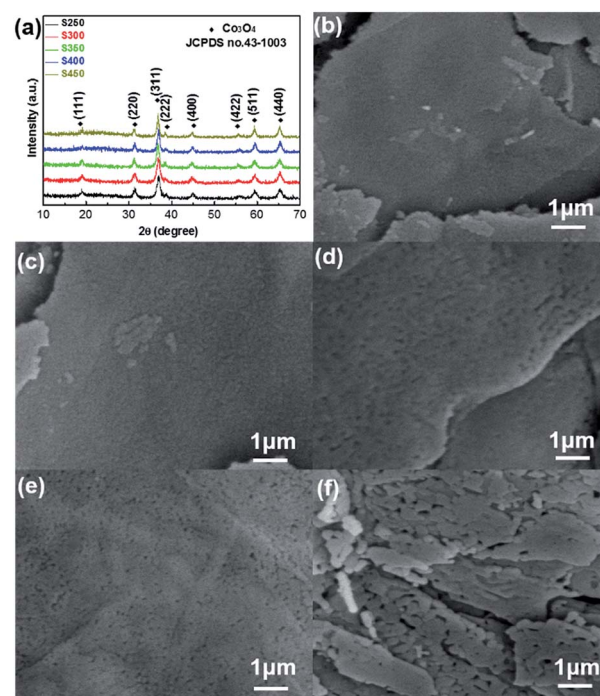


Fig. 3 (a) XRD patterns of S250–S450; (b)–(f) SEM images of Co₃O₄ nanosheets annealed at 250 °C, 300 °C, 350 °C, 400 °C and 450 °C, respectively.

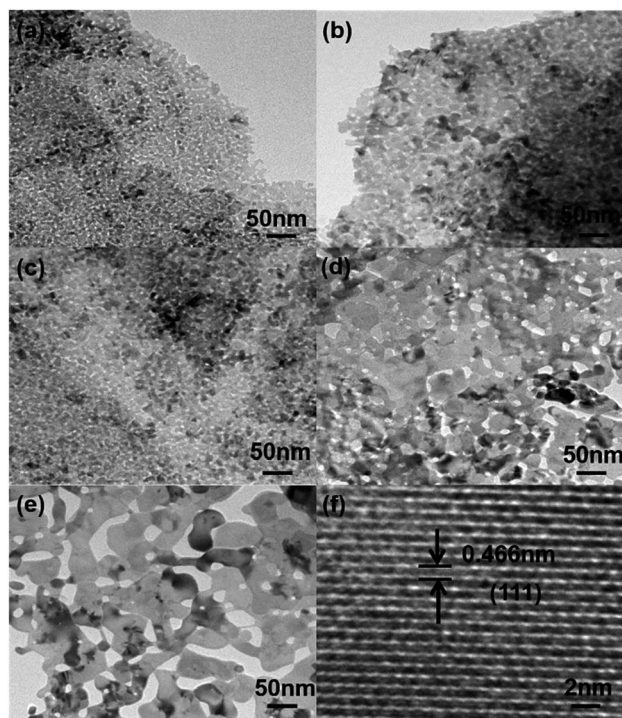


Fig. 4 TEM images of the porous Co_3O_4 nanosheets prepared at different annealing temperatures: (a) 250 °C; (b) 300 °C; (c) 350 °C; (d) 400 °C and (e) 450 °C. (f) HRTEM image of the Co_3O_4 nanostructure annealed at 300 °C.

Fig. 5(b), it is obvious that the distribution of the pore diameter of S300 is more concentrated than others. These results indicate that the morphologies of the Co_3O_4 nanosheets largely depend on the annealing temperature, and controlling the annealing conditions could regulate their microstructures.

Gas sensing properties

The gas sensing properties of the Co_3O_4 mesocrystals with different annealing temperatures were studied with acetone as the probe gas. The Co_3O_4 nanosheets have been uniformly coated on the Ag–Pd finger regions, which provides an electrical path between the neighbouring fingers. Firstly, the acetone sensing characteristics of the above Co_3O_4 nanosheet-based sensors were investigated for an optimum operating temperature. As shown in Fig. 6(a), the optimum operating temperature for both S250 and S300 is 150 °C, while that of S350, S400 and S450 is 170 °C. Among the sensors, S300 exhibited superior sensitivity. The sensitivities of the present sensors were found to increase with the increasing operating temperature, attaining the maximum value (~ 11.4), then decreasing with further increase of the operating temperature. The gas adsorption and desorption kinetics on the surface of Co_3O_4 can be used to explain this behaviour. When the operating temperature is relatively low, the chemical activity of the Co_3O_4 nanosheets is consequently low, leading to a low response. But if the operating temperature increases too much, some adsorbed gas molecules may

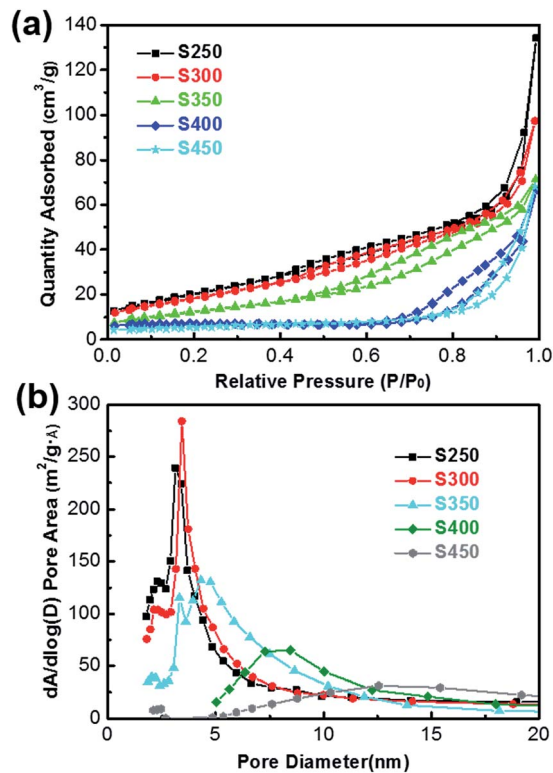


Fig. 5 (a) Nitrogen adsorption and desorption isotherms of the porous Co_3O_4 nanosheets with different annealing temperatures; (b) pore diameter distribution curves of the porous Co_3O_4 nanosheets with different annealing temperatures.

escape from the Co_3O_4 surfaces before the reaction because of the strong thermal motion owing to high temperature, thus responses decrease correspondingly.³⁰ Therefore an appropriate operating temperature is the precondition of the good gas sensing property. The relation curves between the sensors response *versus* acetone with concentrations ranging from 1 to 100 ppm were measured at 150 °C, as shown in Fig. 6(b). As is reported, acetone at concentrations greater than or equal to 1.8 ppm is exhaled from diabetes patients, which are 2–6-fold higher than the 300–900 ppb of acetone exhaled by healthy people.¹⁹ Thus, the acetone detection limit of the sensor was lower than 1.8 ppm and is an important parameter for the applications aimed at the diagnosis of diabetes. This result indicates that this kind of gas sensor can be used to analyse breath acetone for diabetes detection. With the increase of the concentration of acetone, the response also improved rapidly. The response to 100 ppm acetone gas reached ~ 11.4 , which illustrates that the ultrathin Co_3O_4 nanosheet-based sensor not only can be used to detect diabetes but also is useful for other fields which need to detect acetone with high concentration.

Another important parameter of the sensor properties is the response–recovery time, which is calculated under 100 ppm acetone at 150 °C for all samples. Fig. 7(a) shows the response time of S250–S450, decreasing from 150 s to 41 s. And the recovery time of S250–S450 decreases from 300 s to 65 s, as shown in Fig. 7(b).

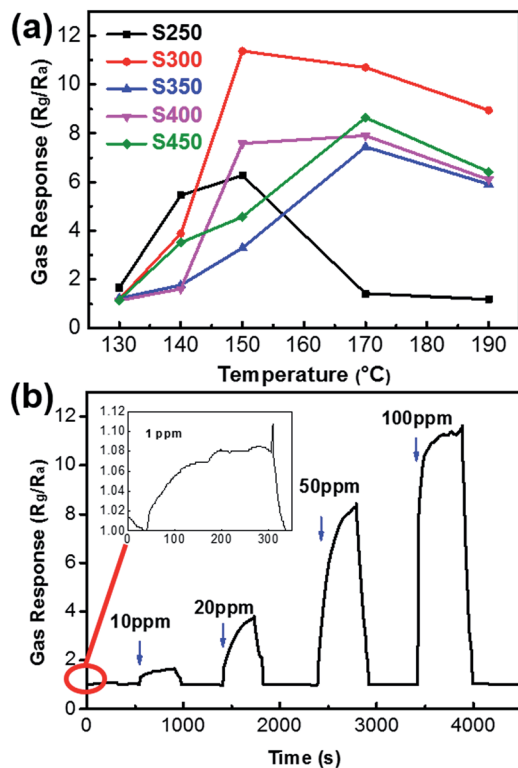


Fig. 6 (a) Gas responses of five samples as a function of different working temperatures to 100 ppm acetone concentration; (b) the response and recovery curves of S300 between different concentrations of acetone gas and air at the operating temperature of 150 °C.

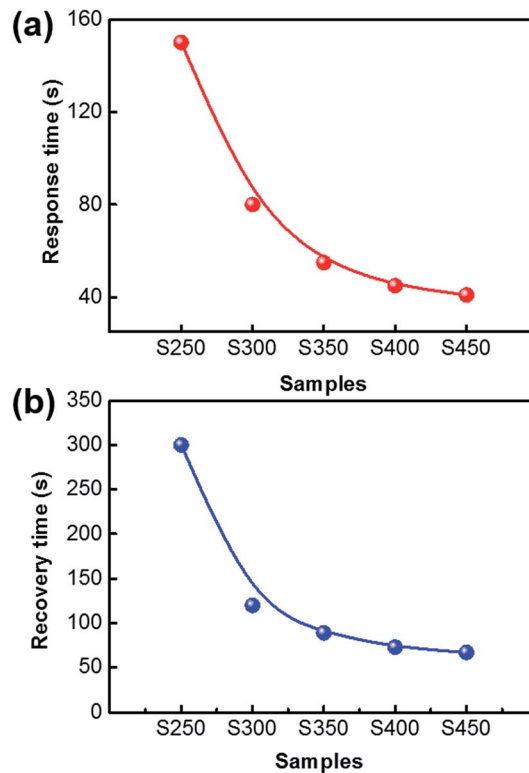


Fig. 7 (a) Response time and (b) recovery time of the samples S250–S450.

Fig. 8 presents the acetone-selective characteristics of S300 with respect to other typical interfering gases such as ethanol, ammonium, methanol, toluene, and *p*-xylene with response values toward each gas at 150 °C. The gas response to 100 ppm acetone vapour is significantly higher than all the other gases at the same concentration, which demonstrates that the sensors based on ultrathin porous Co_3O_4 nanosheets show a high anti-interference performance that is a precondition for becoming a useful sensor to detect breath acetone for diabetes detection. The adsorption ability of ultrathin porous Co_3O_4 nanosheets to some gas molecules, such as acetone, is comparatively stronger than others, which enables it to achieve selective detection.^{31–33}

To confirm the stability of the samples, the responses of S300 at 150 °C to 100 ppm acetone ($\text{RH} \sim 50\%$) were investigated 20 times over two months. The results shown in Fig. 9 illustrate that there was almost no apparent signal attenuation during the 20 tests. Therefore, we can conclude that the stability of this material is good enough to detect acetone over a long time. However, even though this device showed good performance for acetone detection, it does not mean that this device can be directly put into clinical use. There are lots of realistic issues which should be solved first, such as the high humidity levels in breath, fluctuations in humidity and temperature, counteracting volatile compounds in breath, and more.³⁴

Gas sensing mechanism

The gas sensing mechanism for Co_3O_4 widely consists of the change in electrical conductivity when accounting for the chemical interaction of gas molecules with the surface involving gas adsorption, surface reaction, and desorption processes. The schematic diagram of the acetone gas sensing mechanism is illustrated in Fig. 10. Herein, Co_3O_4 is a typical p-type semiconductor, where holes are the main charge carrier. When exposed to air, the oxygen molecules adsorbed on its surface transform to ionized oxygen species (O_2^- , O^{2-} , or O^-) by trapping electrons from Co_3O_4 , forming the depletion layers. When

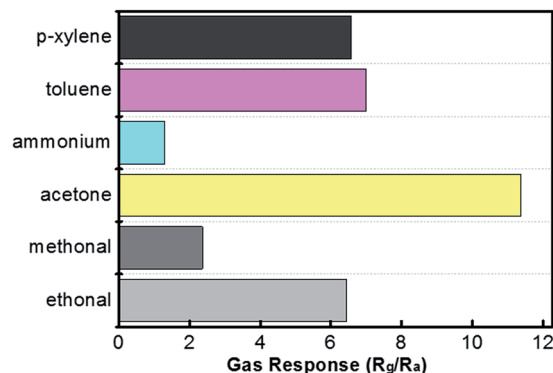


Fig. 8 The gas responses of S300 to several reducing gases with concentrations of 100 ppm at 150 °C.

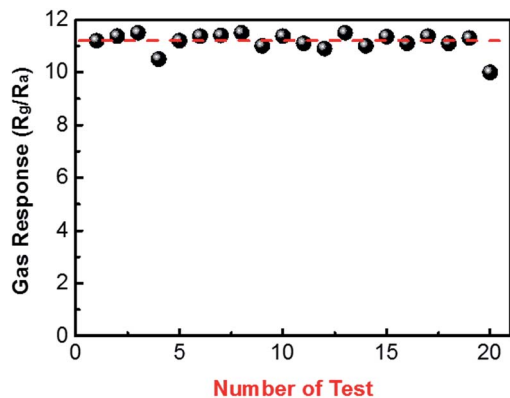
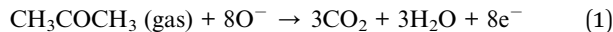


Fig. 9 The response of the Co_3O_4 sensor at $150\text{ }^\circ\text{C}$ to 100 ppm acetone (RH $\sim 50\%$) investigated 20 times over two months.

reductive gas molecules, such as acetone, are introduced into the test chamber, these chemisorbed oxygen species will be released,^{9,35} thus, the charge carrier accumulation layer near the surface is thinned by the electrochemical interaction between O^- and gas molecules, as in the following reaction (1), which releases free electrons and neutralizes the holes in Co_3O_4 , leading to the increase of the baseline resistivity until dynamic equilibrium conditions are obtained. After the acetone flow stopped, oxygen molecules in the air are adsorbed on the surface of the sensors again, and the resistance decreases to its initial value.



In our experiment, we believe that the difference in sensing properties among samples with different annealing temperatures is related to the specific surface chemical composition and microstructure of these gas sensors. As TEM images show in Fig. 4(a)–(e), the nanoparticles in S250 and S300 are smaller than that of S350, S400 and S450, and the pore density of S300 is higher than that of S250. From Fig. 5(a), we can see the corresponding specific surface area of S250 is slightly higher than that of S300. However, from Fig. 5(b), it is obvious that the pore diameter of S300 is bigger than that of S250, and the distribution of the pore diameter of S300 is more concentrated than that of S250. Hence, more oxygen molecules can be adsorbed on the

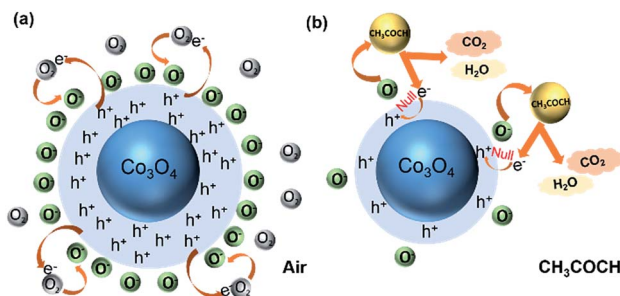


Fig. 10 Schematic diagram of the acetone gas sensing mechanism.

surface of S300 and promote the diffusion of target gases, which are the key factors for the gas sensing properties. Generally, the ultrathin porous structure is beneficial for gas sensing performances, allowing the gas molecules to easily penetrate and adsorb on the surface of the nanosheets and leading to fast response–recovery times as well as high sensitivity.

Conclusions

In conclusion, a gas sensor based on ultrathin porous Co_3O_4 nanosheets has been successfully synthesized through a hydrothermal technique and a subsequent controlled annealing route, showing excellent performances for acetone detection at a much lower operating temperature. The response to 100 ppm acetone reached 11.4 at $150\text{ }^\circ\text{C}$. What's more, the detection limit of Co_3O_4 nanosheet-based sensors is lower than the 1.8 ppm that is exhaled from diabetes patients, and exhibited good reproducibility and stability. Its high-performance is due to the ultrathin structure, meso-porosity, and large specific surface area. These results indicate that the gas sensor based on ultrathin porous Co_3O_4 nanosheets is very promising for making a daily life initial judgment on diabetes in human beings. However, it must be mentioned that there are lots of problems which should be overcome before putting the sensor into practical use.

Notes and references

- 1 P. Spanel and D. Smith, *Med. Biol. Eng. Comput.*, 1996, **34**, 409–419.
- 2 L. Pauling, A. B. Robinson, R. Teranishi and P. Cary, *Proc. Natl. Acad. Sci. U. S. A.*, 1971, **68**, 2374–2376.
- 3 W. Miekisch, J. K. Schubert and G. F. Noeldge-Schomburg, *Clin. Chim. Acta*, 2004, **347**, 25–39.
- 4 A. Damico, C. Dinatale, R. Paolesse, A. Macagnano, E. Martinelli, G. Pennazza, M. Santonico, M. Bernabei, C. Roscioni and G. Galluccio, *Sens. Actuators, B*, 2008, **130**, 458–465.
- 5 D. Hill and R. Binions, *Int. J. Smart Sens. Intell. Syst.*, 2012, **5**, 401–440.
- 6 D. Guo, D. Zhang, N. Li, L. Zhang and J. Yang, *IEEE Trans. Biomed. Eng.*, 2010, **57**, 2753–2763.
- 7 C. Ortiz-Lopez, R. Lomonaco, B. Orsak, J. Finch, Z. Chang, V. G. Kochunov, J. Hardies and K. Cusi, *Diabetes Care*, 2012, **35**, 873–878.
- 8 A. American Diabetes, J. P. Bantle, J. Wylie-Rosett, A. L. Albright, C. M. Apovian, N. G. Clark, M. J. Franz, B. J. Hoogwerf, A. H. Lichtenstein, E. Mayer-Davis, A. D. Mooradian and M. L. Wheeler, *Diabetes Care*, 2008, **31**(suppl. 1), S61–S78.
- 9 J. F. Dummer, M. K. Storer, W. P. Hu, M. P. Swanney, G. J. Milne, C. M. Frampton, J. M. Scotter, G. K. Prisk and M. J. Epton, *J. Breath Res.*, 2010, **4**, 046001.
- 10 A. Kachanov, A. Charvat and F. Stoeckel, *J. Opt. Soc. Am. B*, 1995, **12**, 970–979.

- 11 N. Makisimovich, V. Vorotyntsev, L. N. Nikitin, O. Kaskevich, P. Karabun and F. Martynenko, *Sens. Actuators, B*, 1996, **36**, 419–421.
- 12 M. Phillips, K. Gleeson and R. N. Cataneo, *Lancet*, 1999, **353**, 1930–1933.
- 13 G. F. Fine, L. M. Cavanagh, A. Afonja and R. Binions, *Sensors*, 2010, **10**, 5469–5502.
- 14 T. Akamatsu, T. Itoh, N. Izu and W. Shin, *Sensors*, 2013, **13**, 12467–12481.
- 15 K.-I. Choi, H.-R. Kim, K.-M. Kim, D. Liu, G. Cao and J.-H. Lee, *Sens. Actuators, B*, 2010, **146**, 183–189.
- 16 B. Ding, M. Wang, X. Wang, J. Yu and G. Sun, *Mater. Today*, 2010, **13**, 16–27.
- 17 G. Konvalina, *Acc. Chem. Res.*, 2014, **47**, 66–76.
- 18 H. Haick, Y. Y. Broza, P. Mochalski, V. Ruzsanyi and A. Amann, *Chem. Soc. Rev.*, 2014, **43**, 1423–1449.
- 19 M. Righettoni and A. Tricoli, *J. Breath Res.*, 2011, **5**, 037109.
- 20 L. Liu, S. Li, J. Zhuang, L. Wang, J. Zhang, H. Li, Z. Liu, Y. Han, X. Jiang and P. Zhang, *Sens. Actuators, B*, 2011, **155**, 782–788.
- 21 P. Song, Q. Wang and Z. Yang, *Sens. Actuators, B*, 2012, **173**, 839–846.
- 22 X. Zhou, W. Feng, C. Wang, X. Hu, X. Li, P. Sun, K. Shimanoe, N. Yamazoe and G. Lu, *J. Mater. Chem. A*, 2014, **2**, 17683–17690.
- 23 Z. Wen, L. Zhu, W. Mei, L. Hu, Y. Li, L. Sun, H. Cai and Z. Ye, *Sens. Actuators, B*, 2013, **186**, 172–179.
- 24 Z. Wen, L. Zhu, W. Mei, Y. Li, L. Hu, L. Sun, W. Wan and Z. Ye, *J. Mater. Chem. A*, 2013, **1**, 7511.
- 25 Z. Wen, L. Zhu, Y. Li, Z. Zhang and Z. Ye, *Sens. Actuators, B*, 2014, **203**, 873–879.
- 26 Z. Wen, L. Zhu, Z. Zhang and Z. Ye, *Sens. Actuators, B*, 2015, **208**, 112–121.
- 27 X. Xiao, X. Liu, H. Zhao, D. Chen, F. Liu, J. Xiang, Z. Hu and Y. Li, *Adv. Mater.*, 2012, **24**, 5762–5766.
- 28 X. Liu, J. Zhang, S. Wu, D. Yang, P. Liu, H. Zhang, S. Wang, X. Yao, G. Zhu and H. Zhao, *RSC Adv.*, 2012, **2**, 6178.
- 29 Y. Teng, L. X. Song, L. B. Wang and J. Xia, *J. Phys. Chem. C*, 2014, **118**, 4767–4773.
- 30 S. Wang, C. Xiao, P. Wang, Z. Li, B. Xiao, R. Zhao, T. Yang and M. Zhang, *Mater. Lett.*, 2014, **137**, 289–292.
- 31 L. Li, S. He, M. Liu, C. Zhang and W. Chen, *Anal. Chem.*, 2015, **87**, 1638–1645.
- 32 M. Hakim, Y. Y. Broza, O. Barash, N. Peled, M. Phillips, A. Amann and H. Haick, *Chem. Rev.*, 2012, **112**, 5949–5966.
- 33 B. Wang, J. C. Cancilla, J. S. Torrecilla and H. Haick, *Nano Lett.*, 2014, **14**, 933–938.
- 34 G. Konvalina and H. Haick, *ACS Appl. Mater. Interfaces*, 2012, **4**, 317–325.
- 35 L. Qin, J. Xu, X. Dong, Q. Pan, Z. Cheng, Q. Xiang and F. Li, *Nanotechnology*, 2008, **19**, 185705.